# Raman spectroscopy analysis of human amniotic fluid cells from fetuses with myelomeningocele

Pontiggia, Luca ; Michalak-Micka, Katarzyna ; Hürlimann, Nadine ; Yosef, Hesham K ; Böni, Roland ; Klar, Agnes S ; Ehrbar, Martin ; Ochsenbein-Kölble, Nicole ; Biedermann, Thomas ; Moehrlen, Ueli

DOI: https://doi.org/10.1016/j.yexcr.2024.114048

Experimental Cell Research 439 (2024) 114048

Contents lists available at ScienceDirect

Experimental Cell Research

journal homepage: www.elsevier.com/locate/yexcr

Research article

# Raman spectroscopy analysis of human amniotic fluid cells from fetuses with myelomeningocele

Luca Pontiggia [a,d], Katarzyna Michalak-Micka [a,d], Nadine Hürlimann [a,d], Hesham K. Yosef [e], Roland Böni [h], Agnes S. Klar [a,d,f], Martin Ehrbar [c,f,g], Nicole Ochsenbein-Kölble [c,g], Thomas Biedermann [a,d,f], Ueli Moehrlen [a,b,c,d,f,*]

[a] Tissue Biology Research Unit, Department of Pediatric Surgery, University Children's Hospital Zurich, 8032, Zurich, Switzerland
[b] Spina Bifida Center, University Children's Hospital Zurich, Zurich, Switzerland
[c] Zurich Center for Fetal Diagnosis and Treatment, 8032 Zurich, Switzerland
[d] Children's Research Center, University Children's Hospital Zurich, 8032, Zurich, Switzerland
[e] microphotonX GmbH, 82327, Tutzing, Germany
[f] University of Zurich, 8091, Zurich, Switzerland
[g] Department of Obstetrics, University Hospital of Zurich, Zurich, Switzerland
[h] White House Center for Liposuction, Zurich, Switzerland

ARTICLE INFO

*Keywords:*
Amniotic fluid stem cells
Raman spectroscopy
Spina bifida aperta
Myelomeningocele
cKit/CD117

ABSTRACT

Prenatal surgery for the treatment of spina bifida (myelomeningocele, MMC) significantly enhances the neurological prognosis of the patient. To ensure better protection of the spinal cord by large defects, the application of skin grafts produced with cells gained from the amniotic fluid is presently studied. In order to determine the most appropriate cells for this purpose, we tried to shed light on the extremely complex amniotic fluid cellular composition in healthy and MMC pregnancies. We exploited the potential of micro-Raman spectroscopy to analyse and characterize human amniotic fluid cells in total and putative (cKit/CD117-positive) stem cells of fetuses with MMC in comparison with amniotic fluid cells from healthy individuals, human fetal dermal fibroblasts and adult adipose derived stem cells. We found that (i) the differences between healthy and MMC amniocytes can be attributed to specific spectral regions involving collagen, lipids, sugars, tryptophan, aspartate, glutamate, and carotenoids, (ii) MMC amniotic fluid contains two particular cell populations which are absent or reduced in normal pregnancies, (iii) the cKit-negative healthy amniocyte subpopulation shares molecular features with human fetal fibroblasts. On the one hand we demonstrate a different amniotic fluid cellular composition in healthy and MMC pregnancies, on the other our work confirms micro-Raman spectroscopy to be a valuable tool for discriminating cell populations in unknown mixtures of cells.

## 1. Introduction

Spina bifida (myelomeningocele) is one of the most common neural tube defects with a prevalence of 0.5 per 1′000 of live birth [1]. It is characterized by incomplete closure of the lumbosacral neural tube during the first weeks of pregnancy. As a consequence, the spinal cord remains open and protrudes beyond the level of skin, forming a cystic sac on the back of the fetus. The spinal cord is therefore exposed to chemical and mechanical damage in utero. Today, open fetal-maternal surgery is the gold standard treatment for fetuses with myelomeningocele (MMC) [2,3]. The in utero management of MMC significantly improves the patient's neurological outcome. In individuals with particularly large MMC lesions, autologous skin substitutes would be the ideal approach for closure. To produce stable grafts which ensure better protection of the spinal cord, skin substitutes are presently studied in a sheep model [4,5]. For this, and for future applications in humans, fetal autologous cells, e.g. fibroblasts and keratinocytes, are required. As an alternative to fetal skin biopsies, in recent years amniotic fluid has appeared on the scene as an interesting source of (stem) cells for regenerative medicine, due to the minimal invasive way of isolation and the multipotent properties of some cell subpopulations [6,7].

Of the total number of cells found in the amniotic fluid, only about

* Corresponding author. University Children's Hospital Zurich Department of Surgery Steinwiesstrasse 75, 8032, Zurich Switzerland.
*E-mail address:* Ueli.Moehrlen@kispi.uzh.ch (U. Moehrlen).

https://doi.org/10.1016/j.yexcr.2024.114048
Received 15 February 2024; Received in revised form 11 April 2024; Accepted 13 April 2024
Available online 1 May 2024

10 % consists of viable cells and only one third of them are plastic-adherent colony-forming cells [8]. Among the viable amniotic fluid cells, two population of stem cells have been discovered: amniotic fluid mesenchymal stem cells (AFMSC) and amniotic fluid stem cells (AFSC). AFMSC are isolated by mechanical separation and selection with culture media [9], and show largely mesodermal potential (i.e., they can generate adipogenic, chondrogenic, osteogenic, and myogenic lineages) [10–12], even though a multi-lineage differentiation potential was reported [13,14]. AFSC are isolated through plastic attachment and subsequent CD117 (cKit) selection [15], or directly by CD117 selection of cells from amniotic fluid [16]. AFSC are considered pluripotent [15], or multipotent [14,17,18].

In the second trimester of pregnancy amniotic fluid contains cells that likely originate from the various exfoliating fetal tissues (mainly squamous epithelia) that are in contact with the amniotic fluid, e.g. the skin, the gastrointestinal, respiratory and urinary systems [19]. In addition, congenital malformations can influence the cellular content of the amniotic fluid. For instance', neural tube defects (e.g. spina bifida) contribute neural cells [20], and abdominal wall abnormalities shed peritoneal cells into the amniotic fluid [21].

Given the complexity of the amniotic fluid cellular composition, we believe it is important to investigate the nature of the amniocytes to gain biological useful autologous cells for the construction of skin substitutes.

The aim of this work was to compare the properties of human amniotic fluid cells (AFC) of healthy fetuses and fetuses with MMC by micro-Raman spectroscopy. Micro-Raman microscopy is an emerging tool in regenerative medicine which has the potential to discriminate and classify the type and biochemical status of healthy and pathological cells and tissues in a label-free and non-invasive manner [22–24]. In our study, we found that the MMC and healthy amniotic fluid cell populations can be distinguished by Raman spectral analysis. This is important in view of the identification and isolation of suitable cells for the production of autologous skin grafts for the treatment of defects in fetuses suffering from spina bifida.

## 2. Materials and methods

### 2.1. Human samples

Human fetal skin samples were obtained from fetuses with spina bifida aperta as leftovers during interventions at the University Hospital Zurich. Human amniotic fluid of fetuses suffering from spina bifida was collected during open fetal-maternal surgeries (gestational age 24–26 weeks), human amniotic fluid of healthy fetuses (gestational age 18–20 weeks) was obtained during twin-to-twin transfusion syndrome amnioreduction procedures, in both cases after informed consent of the pregnant women.

Human abdominal subcutaneous adipose tissue samples were obtained from fat lipoaspirates from human healthy donors. The lipoaspirates were performed at the White House, Center for Liposuction Zurich. This study was conducted according to the Declaration of Helsinki Principles and after permission by the Ethics Commission of the Canton Zurich (KEK-ZH-Nr. 2015–0247, BASEC No. PB_2020–00066 and BASEC request No. 2018-00269).

### 2.2. Isolation of cells

Isolation of amniocytes was performed as previously described [15]. In brief, amniotic fluid samples were centrifuged at room temperature for 10 min at 300g. The supernatant was aspirated, and the cell pellet was resuspended in 10 ml of Amniocytes Growing Medium (AGM: high glucose DMEM supplemented with 10 % fetal calf serum (FCS), 1 % sodium pyruvate, and 1 % of penicillin/streptomycin, all ThermoFisher Scientific, Basel, Switzerland). The cell suspension was plated on 10 cm cell culture dishes and the cultures were left undisturbed for 4–5 days to allow appropriate cell adherence. Subsequently, the cells were washed 3 times with Dulbecco's Phosphate Buffered Saline (DPBS, Sigma Aldrich, Buchs, Switzerland) to remove cell debris and fresh AGM was added. The amniocytes were grown in culture at 37 °C and 5 % $CO_2$ until large colonies appeared. The medium was changed every second day. Human adipose derived stem cells (ADSC) were isolated from lipoaspirates as previously described [25,26]. Human fetal fibroblasts were isolated and cultured according to Pontiggia et al. [27].

### 2.3. Fluorescence-activated cell sorting (FACS)

Amniocytes at passage 0 (P0) were harvested using 0.5 % Trypsin/EDTA (ThermoFisher, Basel, Switzerland). Cell suspensions were stained with ZombieAqua Viability Kit (1:600, Biolegend, London, United Kingdom) as well as with cKit-PE antibody (clone 104D2, 1:10, Dako, Baar, Switzerland) for 20 min at 4 °C. After incubation, cells were washed in FACS buffer (DPBS + 0.5 % bovine serum albumin +2 mM EDTA; all ThermoFisher, Basel, Switzerland) and sorted using BD FACSAria™ III Cell Sorter (Flow Cytometry Facility, University of Zurich). The sorted cKit-positive and cKit-negative amniocytes were plated on cell culture dishes and expanded in Amniocytes Growing Medium.

### 2.4. Sample preparation for Raman spectroscopy

Amniocytes, fetal fibroblasts and ADSC were harvested with 0.05 % Trypsin/EDTA, washed in DPBS and counted. 500′000 cells were fixed in 2 % PFA (ThermoFisher) for 5 min at room temperature and washed again twice in DPBS. Eventually, the cells were resuspended in 150 μl DPBS and kept at 4 °C until the analysis was done.

### 2.5. Micro-Raman spectroscopic measurements

Raman measurements were implemented using a platform that combined micro-Raman spectroscopy and laser trapping (Biospex, microphotonX GmbH, Tutzing, Germany) with an inverted microscopic setup. A diode laser of 785 nm wavelength and 120 mW power (TOPTICA Photonics AG, Graefelfing, Germany) is used for Raman excitation. All Raman scattered photons are collected by 60× water immersion objective (1.1 NA, 0.2 WD) (Olympus, Hamburg, Germany) with correction collar set to 0.17 mm. The detection of the Raman scattered photons is achieved using a diffraction grating and a Charge-Coupled Device detector (CCD, Andor, Belfast, UK).

25 μL of PFA-fixed cells in DPBS were pipetted into a sterile μ-channel slide with a 0.17 mm thick borosilicate glass bottom. Approximatively 60 cells from each sample (i.e. from each donor) were randomly selected, measured and 60 spectra were collected randomly from the cytoplasmic or nuclear domain of the cells. Two healthy amniocytes samples from two different donors were measured. The data were merged to in total 115 spectra. In the same way, 7 samples from MMC fetuses were measured and the data were merged to in total 446 spectra.

ADSC and human fetal fibroblasts were isolated from a healthy donor and 30 cells were measured. Cells were exposed to the laser for 30 s to collect a single Raman spectrum. Cells were trapped in the laser focal point during the measurements using optical trapping capability.

### 2.6. Raman data processing

Processing of the spectral data and statistical analysis are performed using MPX-RamSES software (microphotonX GmbH, Tutzing, Germany). All Raman spectra were cropped and analysed to the spectral range of 480–1800 $cm^{-1}$, which contains most of the biological-relevant spectral bands. In Fig. 7 the analysis range was restricted to 600-1700 $cm^{-1}$ to further amplify the relevant spectral regions. This was followed by a baseline correction using an asymmetric least squares fit, cosmic spikes were removed, and the spectra were smoothened with a median filter. The difference between spectra at particular wave-lengths was

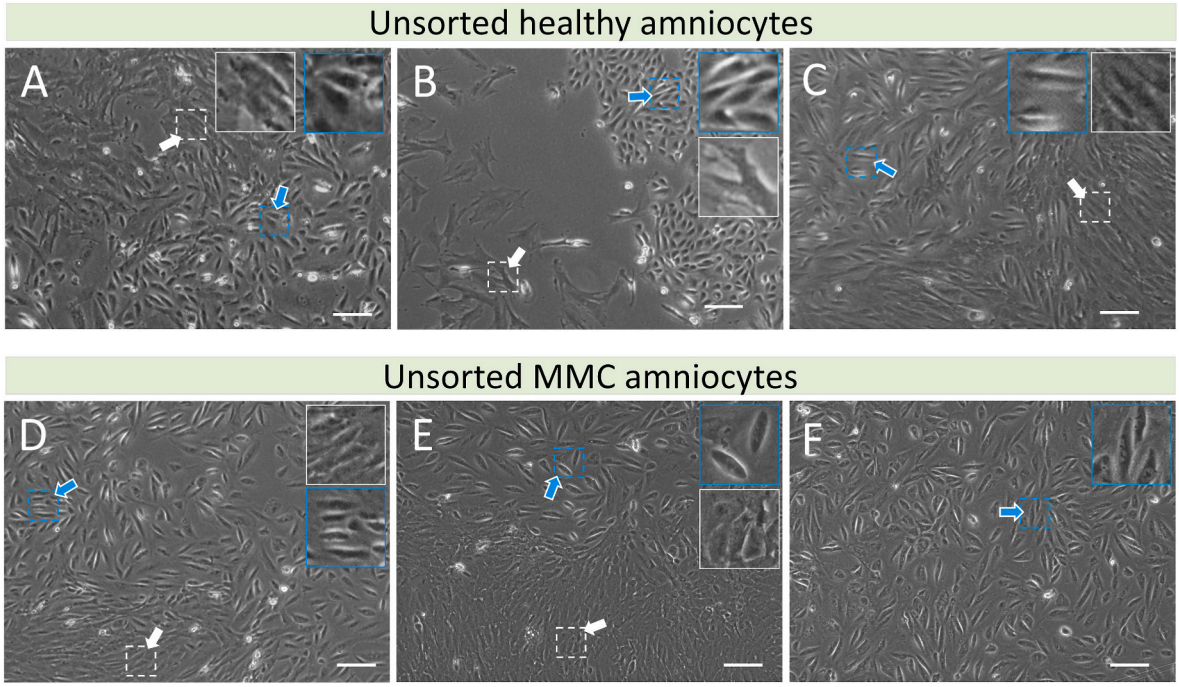


**Fig. 1. Morphological appearance of cultured amniotic fluid cells.** (**A-F**) Representative images of amniocytes isolated from healthy and MMC affected fetuses after two weeks in culture (passage 0) displaying two different morphological cell groups. **(A,B,C)** Healthy amniocytes; **(D,E,F)** MMC amniocytes. Arrows indicate morphological groups: spindle shaped fibroblastoid (white arrows) and cobble stone shaped epithelioid (blue arrows). The inset figures represent the 2.7× magnification of the cells indicated by the arrows. Scale bars: 50 μm.

first estimated manually and reported as "Δ-rating" value in Fig. 2B.

Principal Component Analysis (PCA) was then applied on the datasets. PCA is a statistical method used to reduce the dimensions of large data sets by transforming the large data variables into smaller numbers of components called Principal components (PCs) [28]. The first principal component (PC1) explains for the largest possible variance in the data set (most important variances), the PC2 explains the second most important, etc. The scores of the principal components can be reported as a single plot, 2D-plots (PC1xPC2, etc.) or 3D-Plots (PC1xPC2xPC3). PCA was performed under Python 3, using the scikit-learn package.

PCA Score plots can illuminate the differences and similarities among samples while the PCA loadings display the Raman spectral differences that are used to compare the analysed samples [28,29].

Hierarchical cluster analysis (HCA) was applied as an unsupervised statistical analysis and clustering method to separate the Raman spectra into different groups (clusters) based on the similarity or dissimilarity of the different spectral observations.

Similar to PCA, supervised Linear discriminant analysis (LDA) was applied to characterize differences between samples [30].

## 3. Results

### *3.1. Amniotic fluid cellular compositions from healthy and fetuses with MMC display heterogeneous cell morphology*

Human amniocytes from MMC and healthy amniotic fluid samples were isolated in toto and cultured. After 5–6 days, small cell colonies were visible on the cell culture dish (data not shown). These colonies expanded and exhibited differences in cell morphology. Fig. 1 shows representative examples of amniocytes derived from healthy (A, B, C) and MMC-affected fetuses (D, E, F) after two weeks in culture. In both cases, we observed two different morphological groups: spindle shaped fibroblastoid (white arrows) and cobble stone shaped epithelioid (blue arrows).

### *3.2. Raman spectral analysis of unsorted healthy and MMC derived amniocytes*

At first, we performed micro-Raman spectroscopic analysis of MMC and healthy amniocytes (passage 0). The spectra were recorded in both the cytoplasm and the nucleus of the healthy and MMC cells.

To assess the spectral differences between amniocytes derived from healthy and MMC fetuses, we analysed the mean spectra (Fig. 2A) and the loadings (Suppl. Fig. 1). Only few regions of the spectra showed differences between healthy and MMC samples: region 1 (928-962 $cm^{-1}$), region 2 (1338-1411 $cm^{-1}$), region 3 (1444-1447 $cm^{-1}$), region 4 (1520-1523 $cm^{-1}$).

In general, regions 1, 2, and 4 show molecular features which are more pronounced in healthy amniocytes compared to MMC amniocytes (Fig. 2B, red part of the table). The molecular characteristics of MMC amniocytes are more pronounced in the spectral regions 3 compared to healthy amniocytes (Fig. 2B, blue part). The loadings are presented in Suppl. Fig. 1. Interestingly, the analysis of the PC3 loading plot shows a wavenumber shift at 1447 $cm^{-1}$, which reflects changes in the proteins and lipids composition of the MMC compared to the healthy amniocytes.

In particular, region 1 and 4 (928-962 $cm^{-1}$ and 1520-3 $cm^{-1}$, respectively) contains the spectral contribution of proline and valine (928,936,939 $cm^{-1}$), protein (952,958,961,964 $cm^{-1}$), carotenoids (956/1520-23 $cm^{-1}$) and hydroxyapatite (957,966,960,962 $cm^{-1}$). Also, the C–C backbone of collagen (934 $cm^{-1}$) is represented in region 1.

The spectral region with the most pronounced and significant differences between the MMC and healthy amniocytes is region 2 (1330-1410 $cm^{-1}$), with the contribution of collagen (1338/1344/1401 $cm^{-1}$), tryptophan (1360/1364 $cm^{-1}$), saccharides (1370 $cm^{-1}$), hyaluronic acid (1372 $cm^{-1}$), lipids (1379 $cm^{-1}$), DNA (CH bending and rocking at 1388/1392 $cm^{-1}$), β-carotene (1396 $cm^{-1}$) and aspartate and glutamate (1405-1411 $cm^{-1}$). This spectral region is showing the most significant changes as visualized in the PC1 loading plot, that represent 38.49 % of the variation in the data. (Suppl. Fig. 1). In region 3, we found manly contributions from cholesterol and lipids (1444/1447 $cm^{-1}$), and collagen

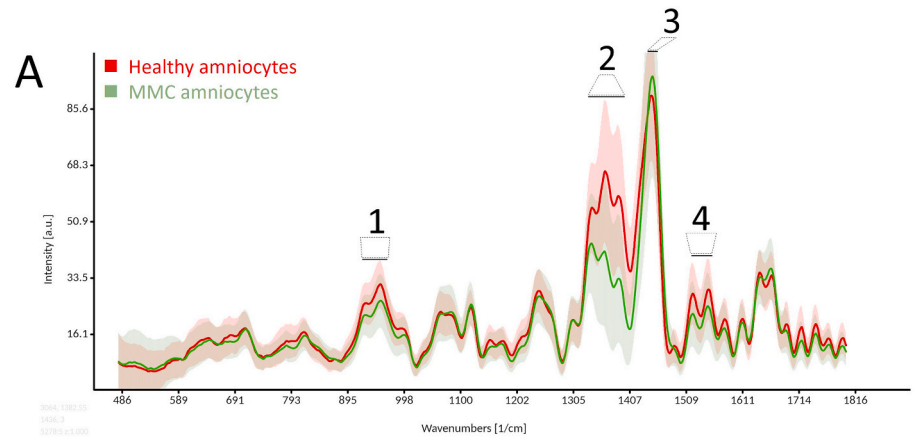


B

| Region | Peak | Assignment | Δ | Origine of cells |
|---|---|---|---|---|
| 1 | 928/936/939 | Proline and valine | | Healty |
| | 934 | Collagen | | |
| | 951 | Protein α-helix | | |
| | 952/958/961/964 | Protein | | |
| | 956 | Carotenoids | | |
| | 957/966 | Hydroxyapatite (HA) | | |
| | 960/962 | Phosphate vibration of HA | | |
| 2 | 1338,1344 | Collagen | +++ | |
| | 1360,1364 | Tryptophan | +++ | |
| | 1370 | Saccharide | +++ | |
| | 1372 | Hyaluronic Acid (CH/CN-def.) | +++ | |
| | 1379 | Lipids | +++ | |
| | 1388,1392 | CH bending, rocking, CN-stretching | +++ | |
| | 1396 | β-carotene | +++ | |
| | 1401 | Collagen | +++ | |
| | 1405-1411 | aspartate and glutamate | +++ | |
| 4 | 1520-23 | Carotenoids | | |
| 3 | 1444 | Cholesterol | | MMC |
| | 1445 | Collagen | | |
| | 1447 | Proteins and lipids | | |

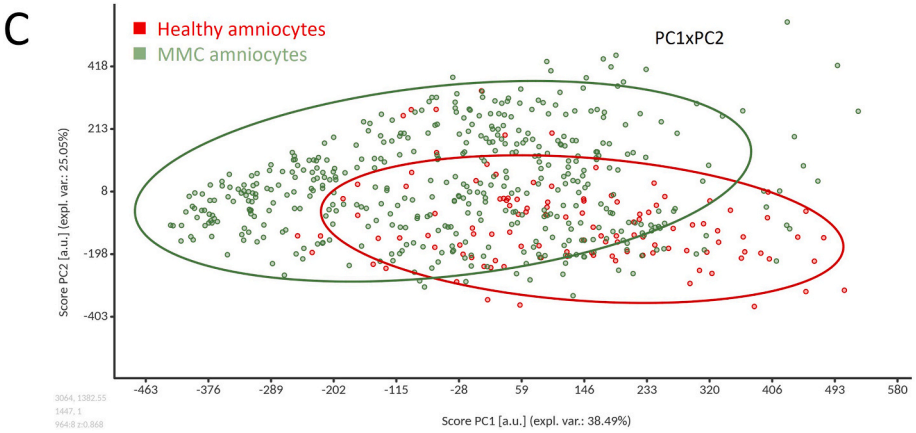


**Fig. 2. Micro-Raman spectroscopy of cultured healthy and MMC amniocytes.** The cytoplasm of 60 randomly selected cells for each sample (MMC: 7 samples, healthy: 2 samples) was analysed with micro-Raman spectroscopy. Measured data from healthy samples were merged to in total 115 spectra, those of MMC samples were merged to in total 446 spectra. (**A**) The mean spectra of MMC samples (in green) and healthy amniocytes (in red) is shown. Shadows represent the standard deviation. 4 spectral regions (1–4) are specified in which the differences are more pronounced (**B**) Possible assignments included in the 4 regions highlighted in A are shown. (**C**) Principal component analysis (PCA) revealing two not clearly distinct populations (overlapping dot clouds). Each dot represents a Raman measurement, and the ellipses describe 90 % confidence interval.

(1445 $cm^{-1}$), and other proteins (1447 $cm^{-1}$). As visible in Fig. 2B, different types of lipids and collagen assignments are present in both healthy and MMC amniocytes, yet the differences (concerning lipids, collagen, but also other molecular attributes) between the MMC and healthy amniocytes cell types are more pronounced and more significant in region 2 (see Δ-rating, in Fig. 2B), where MMC amniocytes show reduced peaks intensities.

We then performed a principal component analysis (PCA): PC1xPC2 scores-plot were used to display the similarity or differences between the healthy and MMC amniocytes (Fig. 2C), based on their Raman spectral data. The first principal component (PC1) explained 38.49 % of the variances in the data set, while the second principal component (PC2) expressed 25.05 % of the variances. The separation of MMC amniocytes from healthy amniocytes was observed over the PC1 axis. The MMC amniocytes scattered over the PC1 positive and negative values, while the healthy amniocytes were spread more homogeneously over the PC1 positive values. A consistent overlap between the MMC and healthy amniocytes in the PC1xPC2 plot was observed. The mean spectra of cultured healthy and MMC amniocytes showed a relative high variance (shadows of the mean spectra in Fig. 2A). This might be due to the heterogeneity of the unsorted amniocytes as shown in Fig. 1A–F.

Raman hierarchical cluster analysis allows to discriminate subpopulations in the heterogenous MMC amniocyte populations.

We showed elsewhere [31] that the exposition of the spinal cord to the amnion fluid during MMC pregnancies could introduce into the amniotic fluid additional (neuronal) cell types which may not be normally present. Thus, we performed first a hierarchical cluster analysis (HCA) of the cultured MMC amniocytes to discriminate possible subpopulations. Fig. 3A shows the processed mean spectra of MMC amniocytes. We performed an unsupervised HCA which classified the data set to three major distinguished groups (Fig. 3B). These groups (clusters) are separated by long vertical lines indicating a more distinct separation (clustering distance). The obtained MMC cell clusters are MMC c1 (137 spectra), MMC c2 (146 spectra) and MMC c3 (163 spectra). The mean spectra of the clusters (putative subpopulations) are shown in Fig. 3C.

The clusters of MMC amniocytes are clearly discriminated in all the spectral regions 1 to 4, with particular efficiency in region 2. However, three additional regions (α, β and γ) show important differences between the putative MMC amniocyte subpopulations (Fig. 3C). In region α, we found the assignments of collagen (1066/1082 cm-1), DNA (1070-72/1094 cm-1), glucose (1071/1074 cm-1) and lipids (1076/1080/1117/1124 cm-1); in region β, amide III (1233-1271 cm-1), lipids and fatty acids (1255/1264 cm-1); Region γ shows the assignment of amide I (1650-1668 cm-1) (Fig. 3D).

Interestingly, MMC c2 and MMC c3 differ only in the regions 2, 3, α

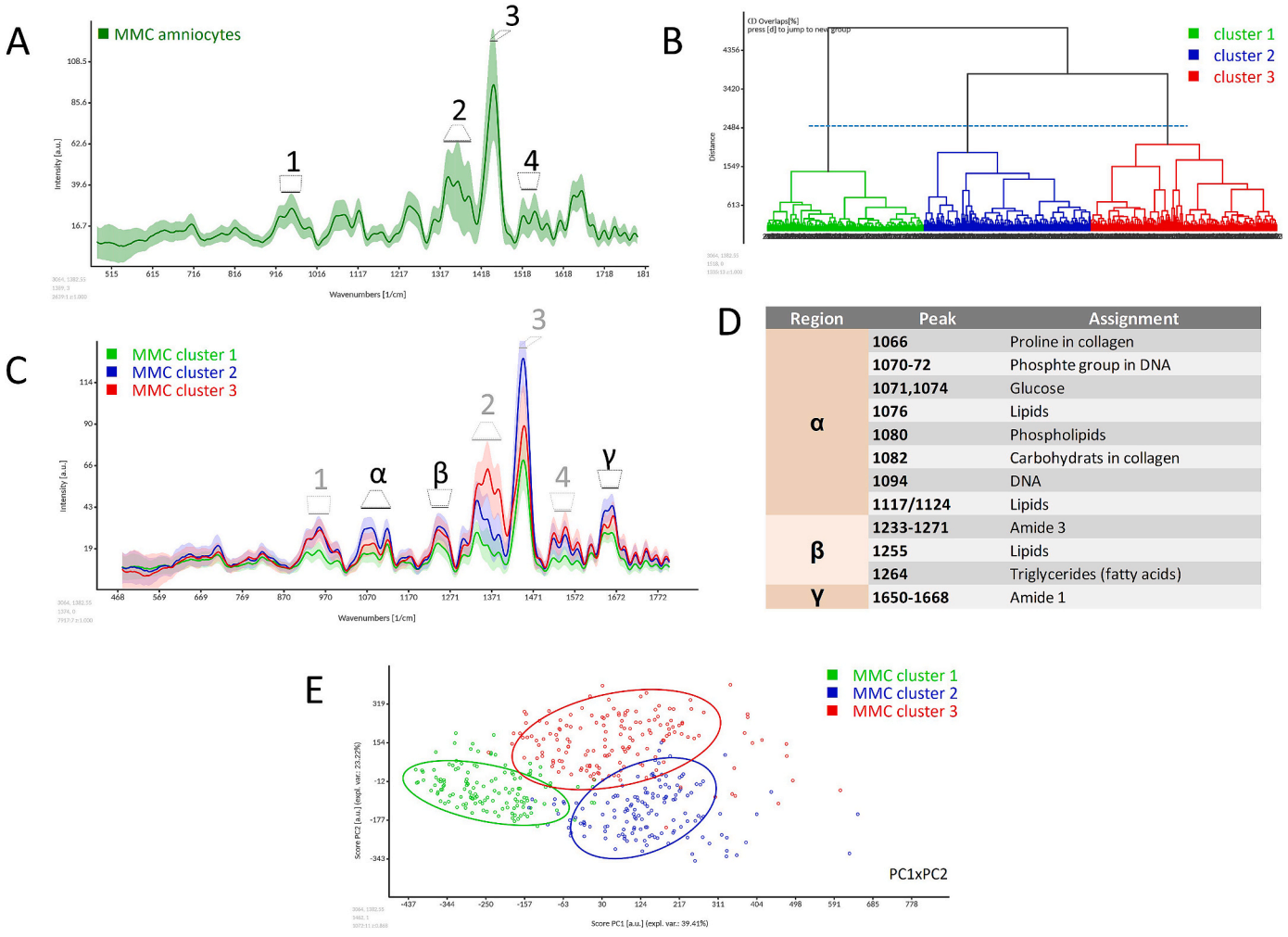


| Region | Peak | Assignment |
|---|---|---|
| α | 1066 | Proline in collagen |
| | 1070-72 | Phosphte group in DNA |
| | 1071,1074 | Glucose |
| | 1076 | Lipids |
| | 1080 | Phospholipids |
| | 1082 | Carbohydrats in collagen |
| | 1094 | DNA |
| | 1117/1124 | Lipids |
| β | 1233-1271 | Amide 3 |
| | 1255 | Lipids |
| | 1264 | Triglycerides (fatty acids) |
| γ | 1650-1668 | Amide 1 |

**Fig. 3. HCA and PCA of MMC amniocytes show potential subpopulations.** Raman analysis of MMC amniocytes. (**A**) The MMC mean spectrum shown in Fig. 2A with the indication of the same assignment regions is shown here alone. Shadows represent the standard deviation. (**B**) HCA of the mean spectra with the visual separation of the identified clusters indicated by the horizontal, dashed blue line. (**C**) Mean spectra of the clusters resulting from the HCA of 3B with the indication the additional assignment regions α, β, γ. (**D**) Possible assignments included in the new regions α, β and γ. (**E**) PC1xPC2 score plots showing the discrimination of the three putative amniocyte subpopulations. Each dot represents a Raman measurement, and the ellipses describe 90 % confidence interval.

and γ, whereas in the regions 1, β and 4 they are very similar. The significance of the discrimination in these regions is visualized with the loading plots (Suppl. Fig. 2), which show in the PC3 the wavenumber shift at 1447 $cm^{-1}$ mentioned above, which reflects changes in the proteins and lipids composition of the MMC cell population. The PC1xPC2 score plots confirm the clear discrimination of the three MMC amniocyte subpopulations (Fig. 3E).

MMC amniotic fluid contains two particular cell populations which are absent in normal pregnancies.

As mentioned above, the discrimination between the putative MMC amniocyte subpopulations can be particularly observed in 7 regions of the mean spectra. In all other regions the spectra are almost identical

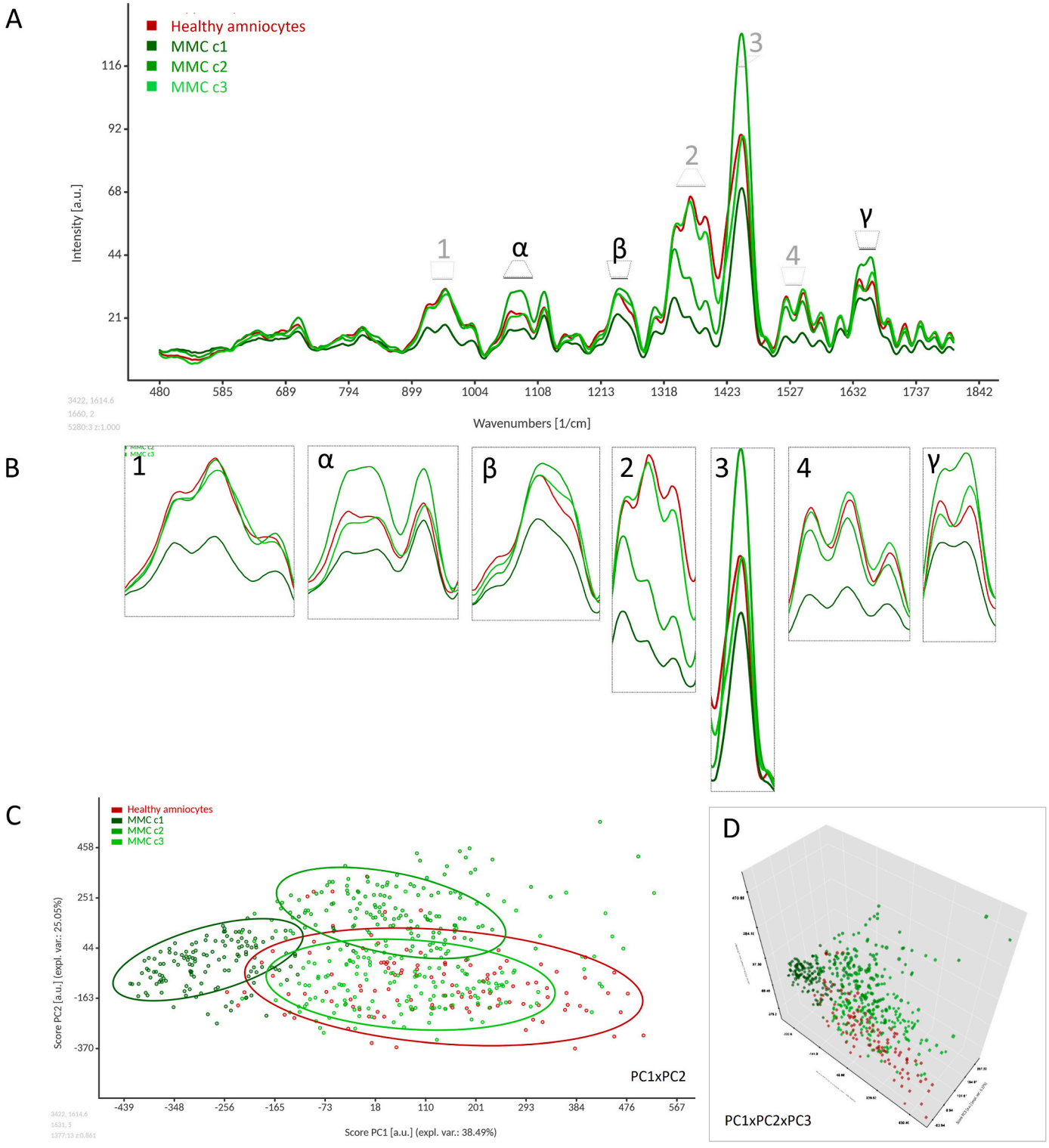


**Fig. 4. PCA of the correlation of putative MMC amniocytes subpopulations and healthy amniocytes.** (**A**) Combined mean spectra of the healthy amniocyte main population (red) and MMC cell clusters (greenish colors) from the HCA shown in Fig. 3C. (**B**) Magnification of the relevant spectral regions from A. (**C**) PCA (PC1xPC2) of healthy main population (red) and MMC (green) putative subpopulations. (**D**) 3D score plot (PC1xPC2xPC3) of the same analysis. Each dot represents a Raman measurement, and the ellipses describe 90 % confidence interval.

(Fig. 3C).

With the additional display of the mean spectrum of the healthy amniocytes, we observed that in these spectral regions always one (c3) or two (c2 and c3) putative MMC subpopulations overlap with the mean spectrum of the healthy amniocytes. MMC c1, in contrast, always differ (Fig. 4A). The magnifications of the relevant spectral regions are shown in Fig. 4B.

Similarly, the PCA shows that the MMC c3-subpopulation completely overlaps with the healthy amniocyte cloud in the PC1xPC2 dot plot (Fig. 4C) whereas MMC c2 displays a reduced and MMC c1 only minimal overlapping area. The 3D-score plot confirms this result (Fig. 4D).

### 3.3. cKit-positive and cKit-negative subpopulations adopt distinct morphologies after sorting

For further characterization of the healthy and MMC amniocytes, we aimed to determine the number of AFSCs present in both types of pregnancies. For this purpose, the cultured amniocytes at passage 0 were sorted for the expression of cKit by FACS. Fig. 5A shows the isotypic control and Fig. 5B the cKit-stained MMC amniocytes. The re-analysis of the sorted populations shows the purity of the sorted cKit-negative (Fig. 5C) and cKit-positive populations (Fig. 5D).

After sorting, cKit-positive and cKit-negative amniocytes were further expanded separately in 2D culture. Interestingly, both cKit-positive and cKit-negative cells exhibited distinct, but in itself homogeneous cell morphologies when cultured in vitro. cKit-positive amniocytes from MMC displayed a fibroblasts-like, elongated, spindle shaped morphology (Fig. 5E). By contrast, cKit-negative amniocytes were smaller and round-shaped (Fig. 5F). The growing behavior of healthy cKit-positive and cKit-negative amniocytes was not remarkably different.

### 3.4. Raman spectroscopy of cKit-positive and cKit-negative amniocytes from healthy and MMC amniocytes

In a next step, sorted and cultured cKit-positive AFSC and cKit-negative cells were analysed by micro-Raman spectroscopy. Fig. 6A shows the mean Raman spectra of cKit-positive and cKit-negative cells from the healthy samples, whereas Fig. 6B illustrates the result with the MMC cells. In both cases, the difference between cKit-positive and cKit-negative was generally not significant, as it can be noted by the strongly overlapping shadows representing the standard deviation. Yet, MMC cells display more pronounced differences in the 7 regions mentioned previously. PCA reflects this result: Fig. 6C shows overlapping healthy

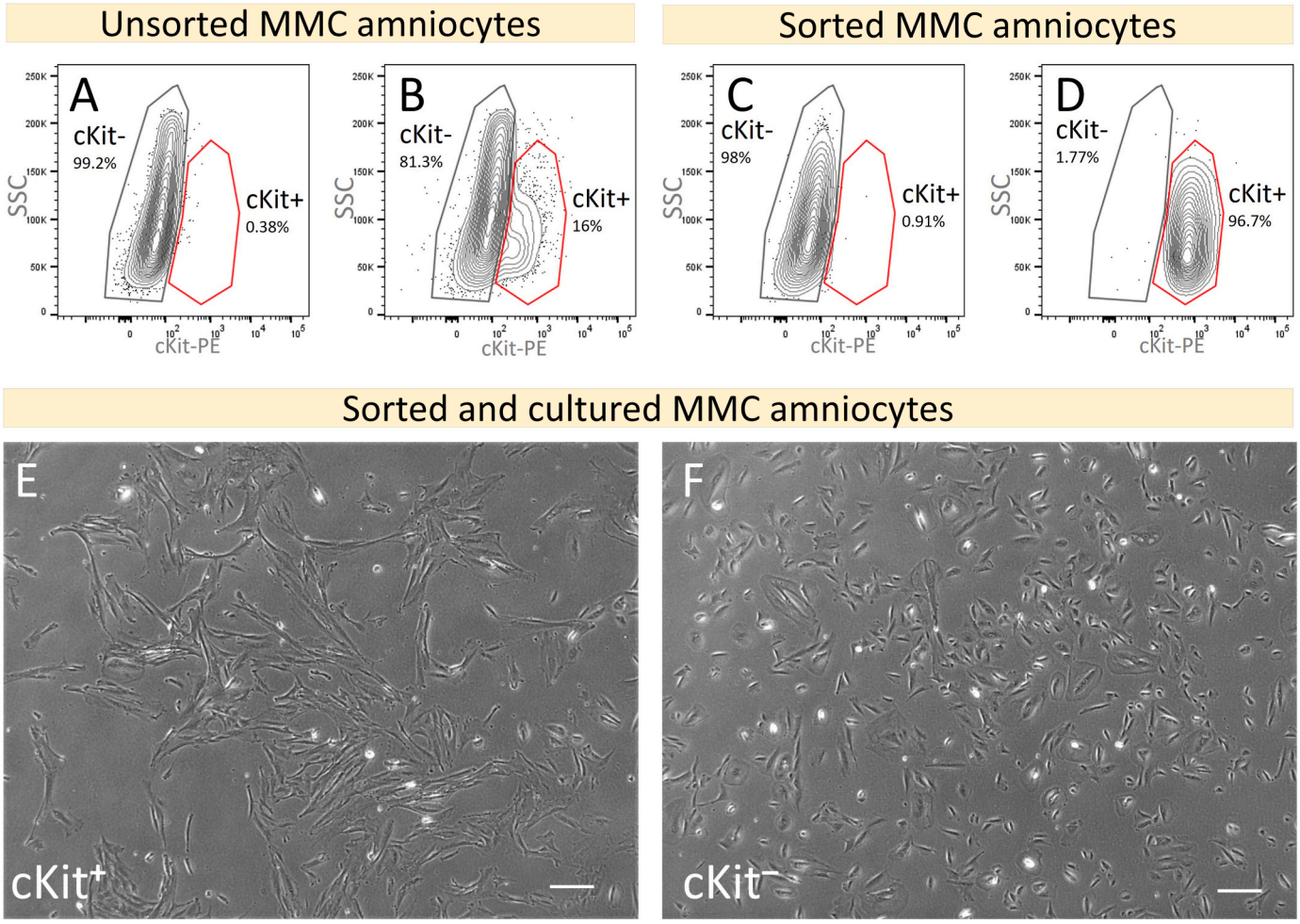


**Fig. 5. Raman spectroscopy of cKit-positive and cKit-negative amniocytes from healthy and MMC amniocyte samples.**
(**A,B**) Flow cytometric analysis of unsorted MMC amniocytes: (**A**) Plot of the isotypic negative control staining: 99.2 % of the cells are included in the "ckit-" gate, no cells (0.38 %) are visible in the "ckit-" gate. (**B**) Plot of the cKit stained sample. Most of the cells do not express cKit (81.3 %) and are visible in the "ckit-" gate. Few cells (16 %) express cKit and are visible in the red "ckit+" gate. The cells in both gates were separately sorted. (**C**) Re-analysis of cKit-negative sorted population. Most of the cells are visible in the "ckit-" gate (98 %). (**D**) Re-analysis of cKit-positive sorted population. The cells (96.7 %) are visible in the "ckit+" gate. Both cKit-positive and cKit-negative cells were plated and cultured separately for one week. (**E, F**) Representative images of amniocytes after sorting (passage 1). (**E**) cKit-positive cells displayed an elongated, spindle-shaped morphology. (**F**) cKit− amniocytes showed a round cell shape. Scale bars: 50 μm.

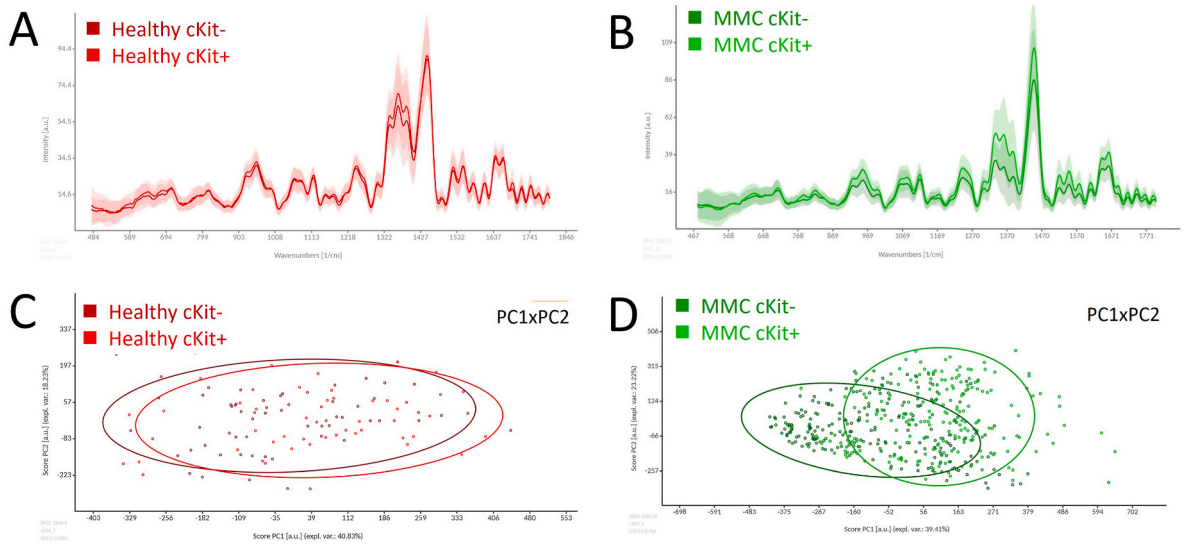


**Fig. 6. Raman spectroscopy of cKit-positive and cKit-negative amniocytes from healthy and MMC amniocyte samples.** (**A**) Mean spectra of cKit-positive and cKit-negative healthy aminocytes. (**B**) Mean spectra of cKit-positive and cKit-negative MMC amniocytes. (**C**) Scatter plot of the PCA of cKit-positive and cKit-negative healthy amniocytes from 2 samples. (**D**) Scatter plot of the PCA of cKit-positive and cKit-negative MMC from 7 samples. From each sample 30 cells were analysed. Each dot represents a Raman measurement, and the ellipses describe 90 % confidence interval.

populations in the PC1xPC2 scatter plot, whereas in Fig. 6D the MMC populations are partially discriminated. Interestingly, in the Suppl. Fig. 3B the MMC loading plot PC3 indicate a wavenumber shift at 1447 $cm^{-1}$ which assign to changes of different proteins and or lipids types (region 3 in Fig. 2) which is absent in the healthy populations (Suppl. Fig. 3A).

Correlation of the molecular fingerprint of human fetal fibroblasts and human adipose derived stem cells with healthy and MMC amniocytes.

In the literature, adipose-derived stem cells (ADSCs) are recognized as promising stem cells in regenerative medicine [32,33], and we successfully isolated them from skin tissue [34], demonstrating their ability to differentiate into various cell types [35].Therefore, for further characterization of healthy and MMC amniocytes, we used ADSCs and human fetal skin derived fibroblasts as reference for stem cells and mesenchymal cells, respectively. Fig. 7A shows the mean spectra of fetal fibroblasts and human ADSC in comparison to the unsorted healthy and MMC amniocyte populations. ADSCs differ from all the cell types in almost all the considered spectral regions (1,3, α,β,γ). Particularly interesting is the characteristic peak of ADSC in region β (grey line) produced from the spectral contributions of lipids and fatty acids (Table in Fig. 3D).

In contrast, the human fetal mesenchymal fibroblasts showed similar mean spectra with the cultured not sorted healthy and cultured not sorted MMC amniocytes (Fig. 7A). The examination of the data through PCA did not resolve the different populations (Fig. 7B). Yet, the elaboration of the data through LDA highlighted the diversity of all the involved cell populations (Fig. 7C). No similarities between the populations could be observed.

We then compared human fibroblasts and ADSC with the sorted healthy and MMC cKit-positive and cKit-negative amniocytes. LDA excludes any correlation of ADSC to healthy or MMC derived cKit-positive and cKit-negative subpopulations (Fig. 7D). This is reflected in the increased distance from all other data sets in the LDA score plot (grey cloud). In contrast, human fetal fibroblasts show similarities with the cKit-negative healthy amniocyte subpopulations (arrow pointed to the dark and dark-red clouds), but not with the MMC populations. The 3D-score plot confirms this result (Fig. 7E).

## 4. Discussion

In the most severe cases of MMC, especially in fetuses with broad defects where the primary surgical closure of the lesion with fetal skin is not feasible, acellular artificial skin matrix, cell-seeded scaffolds or fetal skin substitutes can be used [36–39]. To increase the durability of the substitute covering the lesion and increase the stability of the vertebral column of patients, the addition of a more rigid tissue, such as cartilage, is envisioned [5]. The production of autologous skin-cartilage substitutes implies the isolation of cells from fetal tissues (skin or cartilage) or from the amniotic fluid. Amniotic fluid is an ideal source of stem cells for such applications, due to the minimal invasive way of isolation and the multipotent properties of some subpopulations, amniotic fluid stem cells (AFSC) and amniotic fluid mesenchymal stem cells (AFMSC) [6,14].

In the last decades many efforts have been made to characterize amniotic fluid cells with particular focus on the multipotent stem cell subpopulations [40–42]. Due to their extremely heterogeneous and variable origin, amniotic fluid cells are difficult to be characterized by cell morphological analysis. In the present work, we observed two different morphological groups, called spindle shaped fibroblastoid and cobble stone shaped epithelioid. Other authors also classified amniotic fluid cells in epithelioid, fibroblastic, and “amniotic” [43,44]; or spindle shaped and round shaped [45]; or E-like (epithelial) and F-like (fibroblastoid) cells [46]. Other studies tried to classify amniotic stem cells by RNA or protein profiling providing evidence for the presence of cells expressing mesenchymal, neural and epithelial markers and indicating the existence of progenitor cells with multi-lineage potential [11,41,47].

It is known that congenital malformations can influence the cellular content of the amniotic fluid. Gosden et al., for example, showed that neural tube defects (e.g. spina bifida) or abdominal wall abnormalities contribute neural cells or peritoneal cells, respectively, into the amniotic fluid [20,21]. The presence of additional populations or higher number of (stem) cells in amniotic fluid from fetuses with open neural tube defects was recently confirmed in rodents [48,49].

Since amniotic fluid cells from human fetuses with MMC are still poorly characterized, we applied Raman spectroscopy to analyse and characterize them in comparison to cells derived from healthy individuals. We could highlight a particular Raman spectral region (1330-1410 $cm^{-1}$) which indicates small differences in the cellular

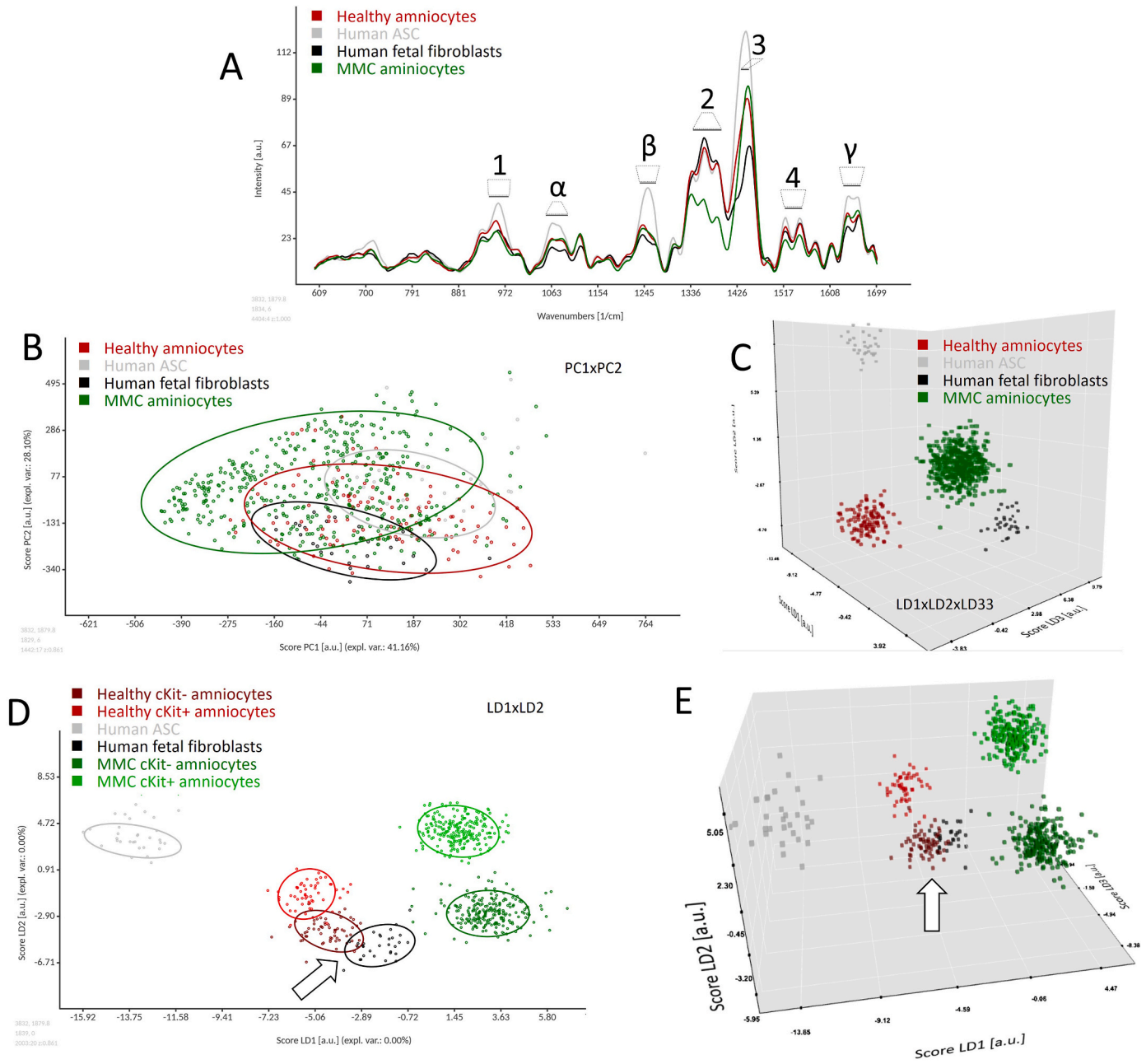


**Fig. 7. Analysis of fibroblasts and ADSC compared to healthy and MMC amniocytes. ADSC and human fetal fibroblasts were isolated from healthy donors and 30 cells per sample were measured.** (**A–C**) Comparison with the healthy and MMC amniocytes presented in Fig. 1. (**A**) Mean spectra with the interested spectral regions 1, 2, 3, 4 and α, β and γ (**B**) 2-dimensional PCA scatter plot. (**C**) 3-dimensional LDA scatter plot. (**D**) Comparison with the sorted healthy and MMC cKit-positive and cKit-negative amniocytes presented in Fig. 6: 2-dimensional LDA scatter plot. Arrows points to the overlapping of human fetal fibroblasts and healthy cKit-negative amniocytes. (**E**) 3-dimensional LDA score plot confirming the overlapping of human fetal fibroblasts and healthy cKit-negative amniocytes (arrow). Each dot represents a Raman measurement, and the ellipses describe 90 % confidence interval.

composition of healthy and MMC derived amniotic fluid samples. In this region the discrimination between healthy and MMC amniocytes was significant as indicated by the PCA and LDA. This reveals differences in the composition of collagen, tryptophan, saccharides, hyaluronic acid, lipids, DNA (CH bending and rocking), β-carotene and aspartate and glutamate.

But what is the link between these particular Raman spectral features and spina bifida?

It is generally assumed that folic acid deficiency, environmental factors, teratogenic exposures (like excess of vitamin A), in addition to chromosome abnormalities or single gene disorders, are common risk factors of spina bifida [50,51]. These agents may influence the molecular characteristic of tissues and cells in the body. For example, during neural tube formation, there is an evidence of glutamic acid decarboxylase expression [52] which may be related with the higher concentration of β-carotene, as a precursor of vitamin A, and glutamic acid in healthy amniocytes in respect to MMC derived. On the other hand, in accordance to our observation, soluble hyaluronic acid and tryptophan were found to be significantly increased in healthy amniotic fluid cells in respect to MMC amniotic fluid cells [53,54]. The contribution to the spectral peaks of the other molecules has to be further elucidated. Yet, as we analysed cells rather than the amniotic fluid itself, it is possible that the particular amniocyte subpopulations which emerged from the HCA in the present work (MMC cluster 1 and 2,

Fig. 4C) could have a relation with the exposed neuronal tissue in MMC which can deliver neuronal cells to the amniotic fluid as mentioned above [31].

In fact, some recent works confirm a higher density of cells from neuronal origin in the MMC amniotic fluid as among the healthy amniocytes. Different authors show by Raman spectroscopy the discrimination between non-differentiated cells (embryonic, mesenchymal or induced pluripotent stem cells) from their differentiated progenies (neural/gut/fibroblast/adipocyte-like cells, chondrocytes or neurons, respectively) [55–57]. Interestingly, the lipid assignments at 1440cm-1 and the amide 1 assignment at 1660cm-1 which display higher peaks in neuronal differentiated cells in the work of Hsu et al. [57], correspond to similar peaks of MMC amniocytes in our work. The healthy amniocytes displayed lower peaks at such assignments. Recently, we also performed single-cell RNA sequencing to characterize the tissue origin and marker expression of cultured MMC amniocytes at the single-cell level. We identified nine different cell types of various origins, mainly from the fetal urogenital tract and the placenta, but also neurons and neuroglia [31]. Thus, we speculate that the MMC cluster 1 and 2 cell populations discriminated by HCA display neuronal properties. Nevertheless, the neuronal origin of these cells will need to be verified in future studies.

Until now we discussed the amniotic fluid cell population as a pool of unknown cell types. Yet, in recent years, there has been a lot of research on amniotic fluid multipotent stem cells subpopulations [6,9,13,58,59]. Amniotic fluid stem cells (AFSCs) are distinguished by the expression of CD117 (cKit) [14].

We could not determine whether AFSCs were present in different numbers in amniotic fluid of healthy and MMC pregnancies. We only observed a convincing spectral identity of cKit-positive and cKit-negative amniocytes in the principal component analysis (PCA) of healthy and MMC amniocytes. The linear discriminant analysis (LDA) showed a weak distinction between the cKit-positive and cKit-negative MMC amniocytes, but surprisingly not between the healthy equivalent populations.

It is necessary to mention a main limitation of our study, which lies in a generally high variance of the data, as it can be noted from the bright SD shadows. We believe that 3 factors contributed to that: The donor variability, the gestational week (in our study 15–25 for healthy and 24–25 for fetuses with MMC) which was shown to significantly influence the presence of stem cells [60,61] and the severity of the MMC defect [14]. Regarding the correlation of amniocytes (n = 2) with ADSCs (n = 1), the small sample size also represents a minor limiting factor.

In conclusion, MMC and healthy amniotic fluid cell populations can be distinguished by Raman spectral analysis and the most discriminating spectral region includes the contributions of collagen and lipids, hyaluronic acid, sugars, tryptophan, aspartate, glutamate, and carotenoids. The difference seems to be related to two particular subpopulations of cells in which the most differences between MMC and healthy cells are clustered. In future, it will be interesting to identify and characterize with other methods the unknown MMC amniocyte subpopulations (referred as cluster 1 and 2 in Fig. 4) which marks an important difference between healthy and MMC samples. It is also conceivable that soon a combination of laser optical trapping with Raman spectroscopy will the opportunity of cell sorting [62]. This will certainly open up new possibilities for characterizing subpopulations through multiple analysis methods such as qPCR, single cell proteomics, FACS and fluorescence microscopy. It will also allow functional analysis, such as the insertion of the separated subpopulations into bioengineered tissues (cartilage, skin) and subsequent transplantation in pre-clinical experiments.

## CRediT authorship contribution statement

**Luca Pontiggia:** Writing – original draft, Visualization, Validation, Methodology, Investigation, Formal analysis, Conceptualization. **Katarzyna Michalak-Micka:** Writing – review & editing, Investigation, Conceptualization. **Nadine Hürlimann:** Investigation, Formal analysis. **Hesham K. Yosef:** Software, Data curation. **Roland Böni:** Writing – review & editing, Resources. **Agnes S. Klar:** Writing – review & editing, Resources, Funding acquisition. **Martin Ehrbar:** Writing – review & editing, Resources. **Nicole Ochsenbein-Kölble:** Writing – review & editing, Resources. **Thomas Biedermann:** Writing – review & editing, Supervision, Resources, Funding acquisition, Conceptualization. **Ueli Moehrlen:** Writing – review & editing, Resources, Funding acquisition, Conceptualization.

## Declaration of competing interest

The authors declare the following financial interests/personal relationships which may be considered as potential competing interests: Hesham K. Yosef is the CSO of microPhotonX GmbH (Tutzing, Germany). For all other authors: No competing interests declared.

## Data availability

Data will be made available on request.

## Acknowledgments

The authors are particularly grateful to the Fondation Gaydoul for their generous financial support. This project has received funding from the Swiss National Science Foundation (SNSF R'equip project no. 316030_205706), Switzerland the Olga Mayenfisch Stiftung, Switzerland and the Fondation Schmieder Bohrisch as well as the Heidi-Ras Stiftung, Switzerland.

Flow cytometry analysis and sorting was performed with equipment maintained by the Center for Microscopy and Image Analysis, University of Zurich.

## Appendix A. Supplementary data

Supplementary data to this article can be found online at https://doi.org/10.1016/j.yexcr.2024.114048.

## References

[1] C.A. Atta, K.M. Fiest, A.D. Frolkis, N. Jette, T. Pringsheim, C. St Germaine-Smith, T. Rajapakse, G.G. Kaplan, A. Metcalfe, Global birth prevalence of spina bifida by folic acid Fortification status: a Systematic review and Meta-analysis, Am J Public Health 106 (2016) e24–e34.

[2] N.S. Adzick, L.N. Sutton, T.M. Crombleholme, A.W. Flake, Successful fetal surgery for spina bifida, Lancet 352 (1998) 1675–1676.

[3] M. Meuli, C. Meuli-Simmen, L. Mazzone, S.J. Tharakan, R. Zimmermann, N. Ochsenbein, U. Moehrlen, In utero plastic surgery in Zurich: successful Use of Distally Pedicled random Pattern Transposition Flaps for Definitive skin closure during open fetal spina bifida repair, Fetal Diagn. Ther. 44 (2018) 173–178.

[4] L. Mazzone, U. Moehrlen, N. Ochsenbein-Kolble, L. Pontiggia, T. Biedermann, E. Reichmann, M. Meuli, Bioengineering and in utero transplantation of fetal skin in the sheep model: a crucial step towards clinical application in human fetal spina bifida repair, J Tissue Eng Regen Med 14 (2020) 58–65.

[5] A. Dasargyri, E. Reichmann, U. Moehrlen, Bio-engineering of fetal cartilage for in utero spina bifida repair, Pediatr. Surg. Int. 36 (2020) 25–31.

[6] A. Bajek, J. Olkowska, N. Gurtowska, T. Kloskowski, M. Walentowicz-Sadlecka, P. Sadlecki, M. Grabiec, T. Drewa, Human amniotic-fluid-derived stem cells: a unique source for regenerative medicine, Expert Opin Biol Ther 14 (2014) 831–839.

[7] K. Rennie, A. Gruslin, M. Hengstschläger, D. Pei, J. Cai, T. Nikaido, M. Bani-Yaghoub, Applications of amniotic membrane and fluid in stem cell biology and regenerative medicine, Stem Cells Int 2012 (2012) 721538.

[8] M.M. Nelson, A.E. Emery, Amniotic fluid cell cultures, J. Med. Genet. 10 (1973) 19–22.

[9] D. Fauza, Amniotic fluid and placental stem cells, Best practice & research, Clinical obstetrics & gynaecology 18 (2004) 877–891.

[10] P.S. In 't Anker, S.A. Scherjon, C. Kleijburg-van der Keur, W.A. Noort, F.H. Claas, R. Willemze, W.E. Fibbe, H.H. Kanhai, Amniotic fluid as a novel source of mesenchymal stem cells for therapeutic transplantation, Blood 102 (2003) 1548–1549.

[11] M.G. Roubelakis, K.I. Pappa, V. Bitsika, D. Zagoura, A. Vlahou, H.A. Papadaki, A. Antsaklis, N.P. Anagnou, Molecular and proteomic characterization of human

mesenchymal stem cells derived from amniotic fluid: comparison to bone marrow mesenchymal stem cells, Stem Cell. Dev. 16 (2007) 931–952.
[12] M.S. Tsai, S.M. Hwang, K.D. Chen, Y.S. Lee, L.W. Hsu, Y.J. Chang, C.N. Wang, H. H. Peng, Y.L. Chang, A.S. Chao, S.D. Chang, K.D. Lee, T.H. Wang, H.S. Wang, Y. K. Soong, Functional network analysis of the transcriptomes of mesenchymal stem cells derived from amniotic fluid, amniotic membrane, cord blood, and bone marrow, Stem cells (Dayton, Ohio) 25 (2007) 2511–2523.
[13] C.R. Harrell, M. Gazdic, C. Fellabaum, N. Jovicic, V. Djonov, N. Arsenijevic, V. Volarevic, Therapeutic potential of amniotic fluid derived mesenchymal stem cells based on their differentiation Capacity and Immunomodulatory properties, Curr. Stem Cell Res. Ther. 14 (2019) 327–336.
[14] S.P. Loukogeorgakis, P. De Coppi, Concise review: amniotic fluid stem cells: the known, the unknown, and potential regenerative medicine applications, Stem cells (Dayton, Ohio) 35 (2017) 1663–1673.
[15] P. De Coppi, G. Bartsch Jr., M.M. Siddiqui, T. Xu, C.C. Santos, L. Perin, G. Mostoslavsky, A.C. Serre, E.Y. Snyder, J.J. Yoo, M.E. Furth, S. Soker, A. Atala, Isolation of amniotic stem cell lines with potential for therapy, Nat. Biotechnol. 25 (2007) 100–106.
[16] A. Ditadi, P. de Coppi, O. Picone, L. Gautreau, R. Smati, E. Six, D. Bonhomme, S. Ezine, R. Frydman, M. Cavazzana-Calvo, I. André-Schmutz, Human and murine amniotic fluid c-Kit+Lin- cells display hematopoietic activity, Blood 113 (2009) 3953–3960.
[17] M. Cananzi, P. De Coppi, CD117(+) amniotic fluid stem cells: state of the art and future perspectives, Organogenesis 8 (2012) 77–88.
[18] S. Joo, I.K. Ko, A. Atala, J.J. Yoo, S.J. Lee, Amniotic fluid-derived stem cells in regenerative medicine research, Arch Pharm. Res. (Seoul) 35 (2012) 271–280.
[19] M.A. Underwood, W.M. Gilbert, M.P. Sherman, Amniotic fluid: not just fetal urine anymore, J. Perinatol. : official journal of the California Perinatal Association 25 (2005) 341–348.
[20] C.M. Gosden, D.J. Brock, Morphology of rapidly adhering amniotic-fluid cells as an aid to the diagnosis of neural-tube defects, Lancet 1 (1977) 919–922.
[21] C. Gosden, D.J. Brock, Combined use of alphafetoprotein and amniotic fluid cell morphology in early prenatal diagnosis of fetal abnormalities, J. Med. Genet. 15 (1978) 262–270.
[22] S. Gomes da Costa, A. Richter, U. Schmidt, S. Breuninger, O. Hollricher, Confocal Raman microscopy in life sciences, Morphologie 103 (2019) 11–16.
[23] S. Rangan, H.G. Schulze, M.Z. Vardaki, M.W. Blades, J.M. Piret, R.F.B. Turner, Correction: applications of Raman spectroscopy in the development of cell therapies: state of the art and future perspectives, Analyst 145 (2020) 2812.
[24] A.C.S. Talari, Z. Movasaghi, S. Rehman, I.u. Rehman, Raman spectroscopy of biological tissues, Appl. Spectrosc. Rev. 50 (2015) 46–111.
[25] A.S. Klar, S. Guven, J. Zimoch, N.A. Zapiorkowska, T. Biedermann, S. Bottcher-Haberzeth, C. Meuli-Simmen, I. Martin, A. Scherberich, E. Reichmann, M. Meuli, Characterization of vasculogenic potential of human adipose-derived endothelial cells in a three-dimensional vascularized skin substitute, Pediatr. Surg. Int. 32 (2016) 17–27.
[26] A.S. Klar, S. Guven, T. Biedermann, J. Luginbuhl, S. Bottcher-Haberzeth, C. Meuli-Simmen, M. Meuli, I. Martin, A. Scherberich, E. Reichmann, Tissue-engineered dermo-epidermal skin grafts prevascularized with adipose-derived cells, Biomaterials 35 (2014) 5065–5078.
[27] L. Pontiggia, T. Biedermann, M. Meuli, D. Widmer, S. Bottcher-Haberzeth, C. Schiestl, J. Schneider, E. Braziulis, I. Montano, C. Meuli-Simmen, E. Reichmann, Markers to evaluate the quality and self-renewing potential of engineered human skin substitutes in vitro and after transplantation, J. Invest. Dermatol. 129 (2009) 480–490.
[28] F. Bonnier, H.J. Byrne, Understanding the molecular information contained in principal component analysis of vibrational spectra of biological systems, Analyst 137 (2012) 322–332.
[29] C. Ricciardi, A.S. Valente, K. Edmund, V. Cantoni, R. Green, A. Fiorillo, I. Picone, S. Santini, M. Cesarelli, Linear discriminant analysis and principal component analysis to predict coronary artery disease, Health Informatics J 26 (2020) 2181–2192.
[30] J. Sulé-Suso, N.R. Forsyth, V. Untereiner, G.D. Sockalingum, Vibrational spectroscopy in stem cell characterisation: is there a niche? Trends Biotechnol. 32 (2014) 254–262.
[31] A. Dasargyri, D. González Rodríguez, H. Rehrauer, E. Reichmann, T. Biedermann, U. Moehrlen, scRNA-seq of cultured human amniotic fluid from fetuses with spina bifida reveals the origin and heterogeneity of the cellular content, Cells 12 (2023) 1577.
[32] L. Mazini, L. Rochette, B. Admou, S. Amal, G. Malka, Hopes and Limits of adipose-derived stem cells (ADSCs) and mesenchymal stem cells (MSCs) in Wound healing, Int. J. Mol. Sci. 21 (2020).
[33] M. Sheykhhasan, J.K.L. Wong, A.M. Seifalian, Human adipose-derived stem cells with Great therapeutic potential, Curr. Stem Cell Res. Ther. 14 (2019) 532–548.
[34] H. Ademi, K. Michalak-Micka, U. Moehrlen, T. Biedermann, A.S. Klar, Effects of an adipose mesenchymal stem cell-derived Conditioned medium and TGF-β1 on human keratinocytes in vitro, Int. J. Mol. Sci. 24 (2023) 14726.
[35] K. Michalak-Mićka, V.L. Büchler, N. Zapiórkowska-Blumer, T. Biedermann, A. S. Klar, Characterization of a melanocyte progenitor population in human interfollicular epidermis, Cell Rep. 38 (2022) 110419.
[36] M. Meuli, C. Meuli-Simmen, A.W. Flake, R. Zimmermann, N. Ochsenbein, I. Scheer, L. Mazzone, U. Moehrlen, Premiere use of Integra™ artificial skin to close an extensive fetal skin defect during open in utero repair of myelomeningocele, Pediatr. Surg. Int. 29 (2013) 1321–1326.
[37] N.A. Hosper, A.J. Eggink, L.A. Roelofs, R.M. Wijnen, M.J. van Luyn, R.A. Bank, M. C. Harmsen, P.J. Geutjes, W.F. Daamen, T.H. van Kuppevelt, D.M. Tiemessen, E. Oosterwijk, J.J. Crevels, W.A. Blokx, F.K. Lotgering, P.P. van den Berg, W. F. Feitz, Intra-uterine tissue engineering of full-thickness skin defects in a fetal sheep model, Biomaterials 31 (2010) 3910–3919.
[38] M. Watanabe, H. Li, A.G. Kim, A. Weilerstein, A. Radu, M. Davey, S. Loukogeorgakis, M.D. Sánchez, K. Sumita, N. Morimoto, M. Yamamoto, Y. Tabata, A.W. Flake, Complete tissue coverage achieved by scaffold-based tissue engineering in the fetal sheep model of Myelomeningocele, Biomaterials 76 (2016) 133–143.
[39] L. Mazzone, M. Pratsinis, L. Pontiggia, E. Reichmann, M. Meuli, Successful grafting of tissue-engineered fetal skin, Pediatr. Surg. Int. 32 (2016) 1177–1182.
[40] I. Virtanen, H. von Koskull, V.P. Lehto, T. Vartio, P. Aula, Cultured human amniotic fluid cells characterized with antibodies against intermediate filaments in indirect immunofluorescence microscopy, J. Clin. Invest. 68 (1981) 1348–1355.
[41] P. Bossolasco, T. Montemurro, L. Cova, S. Zangrossi, C. Calzarossa, S. Buiatiotis, D. Soligo, S. Bosari, V. Silani, G.L. Deliliers, P. Rebulla, L. Lazzari, Molecular and phenotypic characterization of human amniotic fluid cells and their differentiation potential, Cell Res. 16 (2006) 329–336.
[42] M.G. Roubelakis, O. Trohatou, N.P. Anagnou, Amniotic fluid and amniotic membrane stem cells: marker discovery, Stem Cells Int 2012 (2012) 107836.
[43] O. Parolini, M. Soncini, M. Evangelista, D. Schmidt, Amniotic membrane and amniotic fluid-derived cells: potential tools for regenerative medicine? Regenerative medicine 4 (2009) 275–291.
[44] C.M. Gosden, Amniotic fluid cell types and culture, Br. Med. Bull. 39 (1983) 348–354.
[45] F. Vlahova, K.E. Hawkins, A.M. Ranzoni, K.L. Hau, R. Sagar, P. De Coppi, A. L. David, J. Adjaye, P.V. Guillot, Human mid-trimester amniotic fluid (stem) cells lack expression of the pluripotency marker OCT4A, Sci. Rep. 9 (2019) 8126.
[46] C. Pipino, L. Pierdomenico, P. Di Tomo, F. Di Giuseppe, E. Cianci, I. D'Alimonte, C. Morabito, L. Centurione, I. Antonucci, M.A. Mariggiò, R. Di Pietro, R. Ciccarelli, M. Marchisio, M. Romano, S. Angelucci, A. Pandolfi, Molecular and phenotypic characterization of human amniotic fluid-derived cells: a morphological and proteomic approach, Stem Cell. Dev. 24 (2015) 1415–1428.
[47] D.A. Davydova, E.A. Vorotelyak, Y.A. Smirnova, R.D. Zinovieva, Y.A. Romanov, N. V. Kabaeva, V.V. Terskikh, A.V. Vasiliev, Cell phenotypes in human amniotic fluid, Acta naturae 1 (2009) 98–103.
[48] C.G. Turner, J.D. Klein, J. Wang, D. Thakor, D. Benedict, A. Ahmed, Y.D. Teng, D. O. Fauza, The amniotic fluid as a source of neural stem cells in the setting of experimental neural tube defects, Stem Cell. Dev. 22 (2013) 548–553.
[49] E.C. Pennington, K.L. Rialon, B. Dionigi, A. Ahmed, D. Zurakowski, D.O. Fauza, The impact of gestational age on targeted amniotic cell profiling in experimental neural tube defects, Fetal Diagn. Ther. 37 (2015) 65–69.
[50] L.E. Mitchell, N.S. Adzick, J. Melchionne, P.S. Pasquariello, L.N. Sutton, A. S. Whitehead, Spina bifida, Lancet 364 (2004) 1885–1895.
[51] Z. Kibar, V. Capra, P. Gros, Toward understanding the genetic basis of neural tube defects, Clin. Genet. 71 (2007) 295–310.
[52] J.L. Barker, T. Behar, Y.X. Li, Q.Y. Liu, W. Ma, D. Maric, I. Maric, A.E. Schaffner, R. Serafini, S.V. Smith, R. Somogyi, J.Y. Vautrin, X.L. Wen, H. Xian, GABAergic cells and signals in CNS development, Perspect. Dev. Neurobiol. 5 (1998) 305–322.
[53] J. Zieba, M. Walczak, O. Gordiienko, J.A. Gerstenhaber, G.M. Smith, B. Krynska, Altered amniotic fluid levels of hyaluronic acid in fetal Rats with myelomeningocele: understanding spinal cord Injury, J. Neurotrauma 36 (2019) 1965–1973.
[54] A. Kale, E. Kale, The role of amino acids in spina bifida, Clin. Exp. Obstet. Gynecol. 39 (2012) 374–375.
[55] H.G. Schulze, S.O. Konorov, N.J. Caron, J.M. Piret, M.W. Blades, R.F. Turner, Assessing differentiation status of human embryonic stem cells noninvasively using Raman microspectroscopy, Anal. Chem. 82 (2010) 5020–5027.
[56] F. Ravera, E. Efeoglu, H.J. Byrne, Monitoring stem cell differentiation using Raman microspectroscopy: chondrogenic differentiation, towards cartilage formation, Analyst 146 (2021) 322–337.
[57] C.C. Hsu, J. Xu, B. Brinkhof, H. Wang, Z. Cui, W.E. Huang, H. Ye, A single-cell Raman-based platform to identify developmental stages of human pluripotent stem cell-derived neurons, Proceedings of the National Academy of Sciences of the United States of America 117 (2020) 18412–18423.
[58] C. Baughn, S. Campion, S. Elbabaa, Amniotic fluid-derived stem cell potential for therapeutic and surgical use: a review of the literature, Prenat. Diagn. 42 (2022) 157–163.
[59] S. Arnhold, S. Glüer, K. Hartmann, O. Raabe, K. Addicks, S. Wenisch, M. Hoopmann, Amniotic-fluid stem cells: Growth Dynamics and differentiation potential after a CD-117-based selection procedure, Stem Cells Int 2011 (2011) 715341.
[60] S. Da Sacco, S. Sedrakyan, F. Boldrin, S. Giuliani, P. Parnigotto, R. Habibian, D. Warburton, R.E. De Filippo, L. Perin, Human amniotic fluid as a potential new source of organ specific precursor cells for future regenerative medicine applications, J. Urol. 183 (2010) 1193–1200.
[61] S.W.S. Shaw, P.J. Cheng, Y.L. Chang, A.S. Chao, T.H. Wang, S.D. Chang, T.s.T. a. Hsieh, K.H. Chang, Human amniotic fluid stem cells have better potential in early second trimester of pregnancy and can be reprogramed to iPS, Taiwan. J. Obstet. Gynecol. 56 (2017) 770–774.
[62] W.E. Huang, A.D. Ward, A.S. Whiteley, Raman tweezers sorting of single microbial cells, Environ Microbiol Rep 1 (2009) 44–49.